Journal of The Electrochemical Society, **159** (5) B489-B496 (2012)
0013-4651/2012/159(5)/B489/8/$28.00 © The Electrochemical Society

Liquid-Water-Droplet Adhesion-Force Measurements on Fresh and Aged Fuel-Cell Gas-Diffusion Layers

Prodip K. Das,[a] Adam Grippin,[a,b] Anthony Kwong,[a,c,*] and Adam Z. Weber[a,,z]**

[a]*Environmental Energy Technologies Division, Lawrence Berkeley National Laboratory, Berkeley, California 94720, USA*
[b]*Department of Chemical Engineering, University of Florida, Gainesville, Florida 32611, USA*
[c]*Department of Physics, University of California, Berkeley, California 94720, USA*

Optimal water management in proton-exchange-membrane fuel cells at lower temperatures requires the efficient removal of liquid water from the cell. This pathway is intimately linked with liquid-water-droplet removal from the surface of the gas-diffusion layer (GDL) and into the flow channel. In this study, these liquid-water phenomena are investigated experimentally to improve the understanding of water transport through, and removal from, the GDL. Specifically, an experiment using a sliding-angle measurement is designed and used to quantify and measure directly the adhesion force for liquid-water droplets and to understand the droplets' growth and detachment from the GDL. The results show that unlike the static contact angle, the adhesion force, as measured by sliding angles, provides a good indicator of water-droplet removal as it is a direct measure of the dominating force that is holding a droplet on the GDL surface and preventing its detachment. It is also observed that injection through the GDL, as is representative of operating fuel cells, results in a higher adhesion force than a droplet placed on the top surface. Finally, it is shown that aged GDLs demonstrate higher adhesion forces, which dominate GDL degradation response and fuel-cell water holdup.
 [DOI: 10.1149/2.052205jes]

Manuscript submitted December 8, 2011; revised manuscript received February 3, 2012. Published February 28, 2012. This was Paper 783 presented at the Boston, Massachusetts, Meeting of the Society, October 9–14, 2011.

Proton-exchange-membrane fuel cells (PEMFCs) show great promise in becoming energy-delivery devices for a variety of future technologies including stationary power generation and automotive applications. It is well known that water management is a critical component for successful PEMFC operation, especially at low operating temperatures and during startup/shutdown, where liquid water is present.[1–10] Water management is also critical for good PEMFC durability and performance because too little liquid water can cause membrane dehydration and too much liquid water can flood the cathode side of the PEMFC, causing less oxygen to reach the active catalyst sites and consequently decreasing cell performance. Hence, a balanced liquid-water scheme is essential to achieve the full potential of a PEMFC. This scheme invariably involves the existence of liquid water at some point during operation, and removal of it from the cell and into the gas-flow channel (GFC) becomes critically important. This removal is often through liquid-water droplets from the surface of the cathode gas-diffusion layer (GDL) and into the gas stream; understanding this process is essential. Therefore, the subject of liquid-water-droplet detachment from GDL surfaces is a fundamental problem for water transport in PEMFCs and its management. Droplet detachment from a surface is also important for various industrial and chemical processes, such as coating-flow manufacturing processes and enhanced oil recovery. To understand water transport through the GDL, liquid-water removal from the GDL surface, and transport throughout a PEMFC, mathematical and computational modeling has been utilized due to the complex nature of the materials and phenomena. Recently, several reviews have been published exploring the various models for GDL and PEMFC water management.[11–15]

While much progress has been made in modeling transport phenomena in PEMFCs, truly functional and predictive capabilities remain a challenge due to the lack of fundamental understanding of liquid-water transport. Most of the cell-level modeling approaches often rely on empirical correlations between the liquid-water saturation and capillary pressure inside the GDL and neglect the liquid-water droplet growth and detachment from the GDL/GFC interface. Furthermore, liquid-water saturation at the GDL/GFC interface is often considered negligible in the transport models of PEMFCs,[10] while liquid-water droplets form continuously at the GDL/GFC interface. Therefore, droplet growth and detachment from the GDL is not only vital for water management in the PEMFC, but also critical for controlling the transport phenomena throughout the PEMFC.

A significant amount of experimental work devoted to the study of droplet dynamics in PEMFC flow channels has already highlighted some of the fundamental issues.[16–19] Most of these studies, however, are based on Young's equation, which uses the static water-droplet contact angle and its hysteresis of a stagnant droplet placed on top of a GDL. It is worth mentioning that Young's equation applies to ideal surfaces that are perfectly smooth and devoid of all chemical and structural inhomogeneities. The contact angle measured on a rough surface, like a PEMFC GDL, called the Wenzel angle, θ_W, does not obey Young's equation; it is related to the equilibrium Young angle, θ_Y, by [20]

$$\cos\theta_W = r\cos\theta_Y \quad [1]$$

where r is the roughness factor that represents the ratio of the true wetted area to the superficial surface area. In addition, Eq. 1 only applies to equilibrium angles on rough surfaces and not to advancing and receding angles that give rise to contact angle hysteresis.[21] Conversely, PEMFC GDLs are not only rough, but also chemically inhomogeneous due to the nonuniform distribution of binding material and Teflon (which is used to improve GDL's hydrophobicity) as shown in Figure 1. Figure 1a shows a scanning-electron-microscope image of a Sigracet carbon-paper GDL (SGL Technologies GmbH, Meitingen, Germany) without Teflon loading, and Figure 1b shows the image of a GDL with 20-wt% Teflon. Therefore, the wettability and spreading of a water-droplet and its movement on the GDL surface will be sensitive to the GDL's chemical and structural inhomogeneity, and the direct use of Young's equation for such surfaces is questionable.[22–25]

The sliding angle, which is a measure of droplet mobility and detachment from a surface, is often estimated using a theoretical relation between the sliding angle and the contact angle hysteresis,[26,27] although it is known that the contact-angle hysteresis is more qualitative than rigorously quantitative in terms of droplet mobility.[28] This hysteresis is defined as the difference between the advancing and receding contact angles, $\theta_a - \theta_r$; an illustration of these angles is shown in Figure 2. Figure 2a shows the static contact angle, θ_c, and the surface-tension forces for a liquid-water droplet on a solid surface, and Figure 2b shows the advancing, θ_a, and receding, θ_r, contact

* Electrochemical Society Student Member.
** Electrochemical Society Active Member.
z E-mail: azweber@lbl.gov

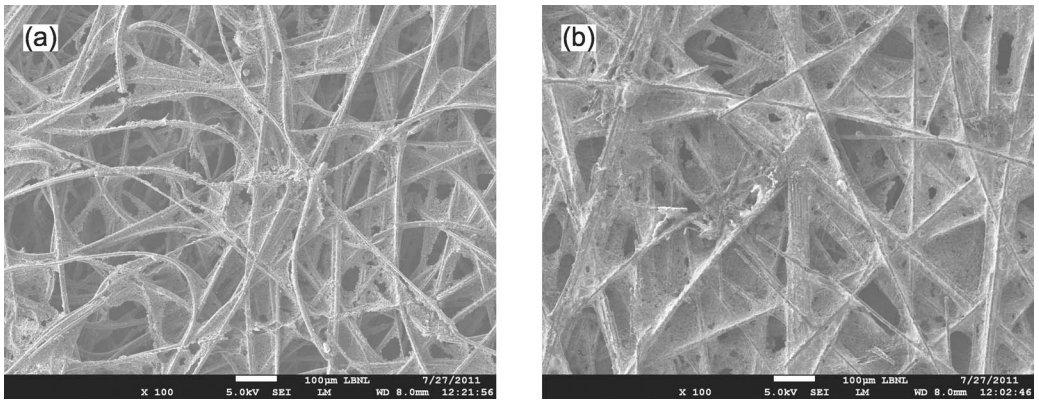

Figure 1. Scanning-electron-microscope images of PEMFC GDLs showing surface inhomogeneity both without (a) and with (b) Teflon loading.

angles, and the sliding angle, θ_s. The sliding angle, also known as the roll-off angle, indicates the angle of inclination of a surface when a droplet completely rolls off of the surface due solely to gravity. The resistance force (known as the adhesion force) that the droplet needs to overcome during the slide is shown in Figure 2c for a homogeneous surface. It should be noted here that the contact area between a droplet and an inhomogeneous rough surface, such as PEMFC GDLs, will always be asymmetric. From Figure 2, one can see that the advancing and receding contact angles measured on a level surface are not rigorously valid for predicting sliding angles for an inclined rough surface.[29] However, the advancing and receding contact angles can be correlated with the sliding angle if the length scale and shape constant for the contour of the droplet are known.[27] Since PEMFC GDLs have both chemical and structural inhomogeneity, a droplet's length scale and shape constant are difficult to quantify experimentally. While the static contact angle and contact-angle hysteresis can provide insight into the liquid-droplet movement on a smooth solid surface, the correct identification of the contact angles at the edges of the drop can be extremely difficult on an inclined surface.[30–32]

Several studies have also shown that the dynamic behavior of water droplets is strongly affected by the surface roughness (even on a scale of around 10 nm) and the history of the surface.[33–35] Hence, the contact-angle hysteresis is not a good index of dynamic hydrophobicity for liquid-water droplets on a porous and chemically inhomogeneous PEMFC GDL. Furthermore, liquid water in a PEMFC is transported from the catalyst layer to the GDL; hence, the pinning effect is expected to have a strong influence on droplet movement along the GDL surface. The pinning effect represents the droplet's behavior when the liquid-gas interface of the droplet shrinks without shrinking or moving the solid/liquid contact line, and it maintains its initial position. Therefore, the solid/liquid contact line behaves as it is pinned to the solid surface.[36] It might be impossible to avoid the pinning effect for a droplet size of 1 mm or smaller, which is the typical droplet size for PEMFCs, since it is the same as typical flow-channel dimensions. Furthermore, contact-angle hysteresis does not provide an accurate estimation of the adhesion force between the liquid-water droplet and GDL surface. Therefore, a direct measurement of the sliding angle is key to understanding liquid-water droplet movement and detachment from the PEMFC gas-diffusion layer.

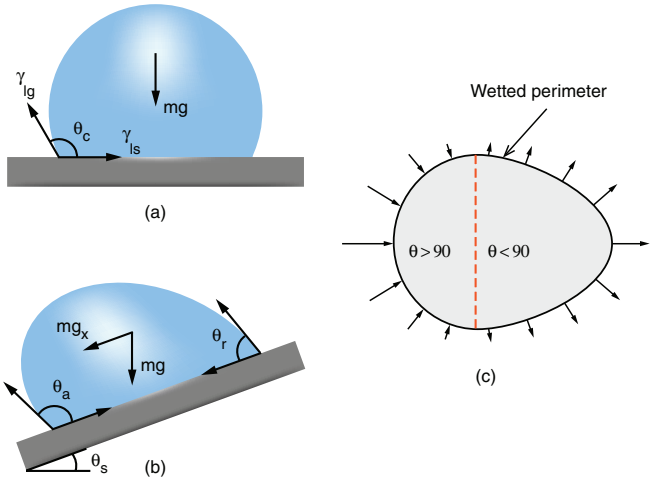

Figure 2. Illustration of contact angles and forces acting on a liquid water droplet on a solid surface. (a) Static contact angle (θ_c) with the body force (mg) and surface tension forces (γ_{lg} and γ_{ls}). (b) Advancing (θ_a) and receding (θ_r) contact angles and sliding (roll-off) angle (θ_s). (c) Top view of the adhesion force distribution that is preventing the droplet from roll-off (parallel to the solid surface); dashed line shows contact angle transition through 90°.

In this study, we have designed and used a tilted-surface experiment to quantify and measure directly the sliding angles and adhesion forces for liquid-water droplets on various GDL surfaces. As shown in Figure 2, at the incipient sliding angle, the adhesion and gravity forces acting on the liquid-water droplet equal each other. Thus, one can calculate the adhesion force between the liquid-water droplet and GDL surface from the body force acting along the direction of the slide and the wetted diameter,

$$F_{\text{adhesion}} = \frac{\rho V g \sin\theta_s}{\pi d_w} \qquad [2]$$

where ρ is the water density, V is the droplet volume, g is the gravitational acceleration constant, θ_s is the sliding angle, and d_w is the wetted diameter. The wetted diameter represents the equivalent diameter of the wetted area between the droplet and GDL surface (see Figure 2).

In this paper, the technique is examined and different aspects of the technique and liquid-water-droplet growth and detachment from the GDL surfaces are explored. These aspects include the effect of droplet formation and injection method and rate. Finally, the water and water-droplet characteristics of ex-situ aged GDLs are explored and compared to fresh samples to ascertain the impact of aging.

Experimental

The experimental measurement of sliding angles was performed using a modified automated Goniometer (ramé-hart model 290) with a custom-made injection system. The experimental setup with its key components is shown in Figure 3. A detailed description of the experimental apparatus and measurement procedure are given in the following paragraphs.

Apparatus.— The liquid-water-droplet profile images were taken using a CCD camera with 7 mm × 5 mm field of view (640 × 480 pixels) at half-second time intervals; droplets were backlit with a

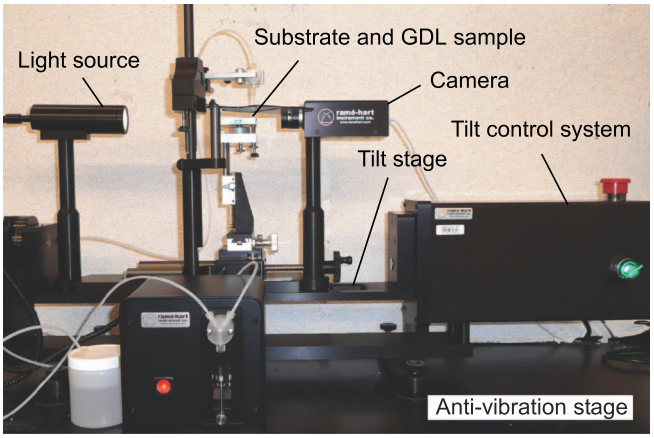

Figure 3. Setup used in the tilted-surface experiment to measure sliding angles and adhesion forces for GDL surfaces.

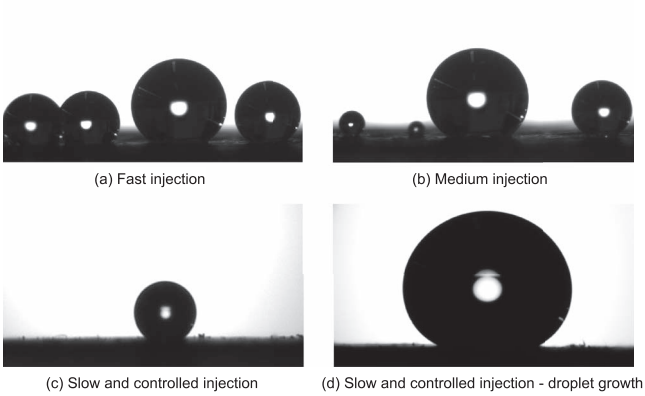

Figure 4. Effect of injection rate on the creation of liquid-water droplets on SGL 24DA GDL for bottom injection method.

diffused 150 W halogen lamp. The camera was mounted to a stage that was inclined by a rotary motor at a constant angular speed (the rotary motor can operate as low as 0.1°/s). Movement of the stage was vibration-free with no backlash and vibrations from surroundings were isolated from the stage using an anti-vibration stage to ensure that the liquid-water droplet releases only due to gravity.

Injection methods and drop creation.— Liquid-water droplets on Sigracet carbon-paper GDLs (SGL GDLs) were placed using two injection methods (on the top and through the bottom of the GDL sample) and two placement methods (placed on a horizontal surface and placed on a pre-tilted surface). A list of Sigracet carbon-paper GDLs that were tested in this study is given in Table I. For top injection, a porous GDL sample was attached with a solid substrate and then a fixed volume of liquid water was injected using an automated dispensing system with a constant injection rate. Therefore, the top injection was a deposition method, where the droplet was deposited on top of a horizontal GDL sample using an injection system placed above the GDL sample. The optimum injection rate was determined using several measurements. For smaller drops, it was found that the sliding-angle data were statistically consistent for the injection rate of 2 μL/s or lower. Therefore, a rate of 2 μL/s was used for the 5 μL droplets and for larger drops a rate of 1 μL/s was used, which ensures that the dynamic effect of droplet creation is minimal. Once a droplet reached the desired volume, the entire stage was inclined at a constant speed until the droplet completely rolled-off from the GDL surface.

The bottom injection method was designed to mimic liquid-water-transport process in a PEMFC cathode where liquid water is produced in the catalyst layer and transported through the GDL, eventually appearing as droplets at the GDL/GFC interface. In this case, the GDL sample was attached with a pre-drilled solid-substrate to allow liquid water to flow through the bottom of the GDL. Liquid water was then injected through the bottom of the sample at a constant injection rate until the desired volume was reached. The injection speed was also critical to ensure the growth of only one droplet within the viewing window of the camera (~7 mm wide), as illustrated in Figure 4. As shown in Figure 4a, multiple droplets formed and grew in a 7 mm-wide region for an injection rate of about 20 μL/s, while at a lower injection rate, multiple droplets were also formed but only one grew continuously as shown in Figure 4b. Conversely, a slower injection rate (usually 1 μL/s or less) always showed growth of only a single droplet as shown in Figure 4c and 4d. Furthermore, the droplet volume and total injection volume were not equal for the bottom injection because of the porous nature of the GDL; the droplet volume was always less than the injection volume. Therefore, the volume of the droplet was first measured to ensure it reached the desired volume, and then the stage was inclined at a constant rate (mostly between 0.5°/s and 1°/s) depending on the droplet size, until the droplet completely rolled-off from the GDL surface.

It was observed that the addition of kinetic energy due to the angular motion of the stage is significant for a water droplet larger than 10 μL. For example, a 20 μL droplet on SGL 24DA (20-wt% Teflon loading) GDL showed sliding angles of 4.62° and 6.62° for angular speeds of 1°/s and 0.5°/s, respectively. Conversely, a 5 μL droplet showed almost identical sliding angles for both speeds. Since the increase of droplet mass is four times for a 20 μL droplet, the angular speed was reduced to half to minimize the addition of kinetic energy. Therefore, for smaller drops an angular speed of between 0.5°/s and 1°/s was used, and for larger drops an angular speed of 0.5°/s or less was used to reduce the effect of the stage's angular motion.

Two placement methods were also investigated: post-tilt and pre-tilt. In the post-tilt method, a liquid-water droplet of a given volume was created on a horizontal surface and then the instrument was rotated. Both top and bottom injections were used for post-tilt. For the pre-tilt method, the instrument was first tilted and then a droplet was created using bottom injection, and the volume noted when it rolled-off. It was found that for large droplets (>10 μL), the sliding angles are higher for droplets created on a horizontal surface than the droplets created on a pre-tilted surface. For small droplets, the sliding angles are almost identical or slightly higher for the pre-tilt method. A possible reason for this situation is that there is additional kinetic energy added due to the injection rate in the pre-tilt method. It was decided to use only the post-tilt method in this study.

To obtain statistically significant results, several measurements were taken for each data point in terms of both locations on the GDL and number of injections. Eight to ten measurements were taken within 5% (or less) of the desired volume, and then the average and standard deviation of the sliding angles were calculated. Each measurement was entirely software controlled (DROPimage) and automated to ensure consistency for all the injection and placement methods. It should also be noted that the history of a GDL can also impact the sliding-angle measurements as a previously tested GDL (one day of use and left overnight uncovered) shows about 10 to 20% higher sliding angles

Table I. Teflon loading in tested Sigracet (SGL) carbon-paper GDLs.

Type	Teflon loading (wt%)
SGL 24AA	0
SGL 24BA	5
SGL 24CA	10
SGL 24DA	20
SGL 24EA	30

than an untested GDL even after one day of use. This aspect is explored in more detail in the aging analysis.

Results and Discussion

In this section, the estimation of the adhesion force for GDL surfaces and the impacts of injection method, injection rate, and GDL aging on the sliding angles are discussed. The issues of the technique viability and contact angles, especially in context to rough and smooth surfaces and prior studies, are addressed above in the Introduction.

Impact of injection method.— As already mentioned, the sliding angle for a liquid-water droplet on the GDL surface has to be determined experimentally for macroscopically calculating the adhesion force as a function of droplet volume. Figure 5 shows the measured sliding angles for liquid water droplets on SGL 24DA GDL for the two injection methods: top and bottom. Here, the symbols represent the measured data with standard deviation, while the lines are exponential fits, which for the top- and bottom-injection methods are

$$\theta_{s,t} = 22.547e^{-0.077\,V}, \quad R^2 = 0.998 \qquad [3]$$

and

$$\theta_{s,b} = 70.847e^{-0.052\,V}, \quad R^2 = 0.995 \qquad [4]$$

respectively, where V is the droplet volume in μL. Note that the sliding angle data reported in this study represent complete roll-off from the GDL surface.

It is worthwhile to note that the diameter of a 5 μL droplet is about 1.75 ± 0.25 mm depending on the GDL's hydrophobicity, whereas typical PEMFC flow channels are between 1 to 2 mm wide. Therefore, the fitted curves allow extrapolating sliding angles for droplet size smaller than 5 μL, which are relevant to PEMFCs. Of course, this extrapolation is expected to increase in error as the droplet size approaches that of the pores and fibers comprising a GDL; however, such small sizes are not expected during PEMFC operation. The reason why all the measurements were done for the droplet size of 5 μL and higher is so that gravity will be strong enough to make the droplet roll-off at a reasonable angle. The variation of the gravity body force and the adhesion forces for water droplets on the SGL 24DA GDL are shown in Figure 6. Here the gravity force is approximated from the droplet volume and static-contact-angle data. As shown in Figure 6, the droplet diameter has to be over 1 mm for top injection and over 1.75 mm for bottom injection to overcome the gravity force.

The average static contact angles (not shown) for top and bottom injections for SGL 24DA are found to be almost identical for a given droplet volume, whereas the droplets placed using a bottom-injection method have consistently higher sliding angles than those placed using a top-injection method. This trend cannot be attributed to the addition of kinetic energy in the top-injection method due to the large variation observed in Figure 5. For example, the contribution to adhesion force due to the addition of kinetic energy for a 20 μL droplet is observed to be about 1 mN/m. Since liquid water can flow through multiple pores of the GDL while injecting through the bottom of the GDL, liquid columns are formed underneath the droplet and assist the droplet's adhesion, thereby preventing it from detaching from the GDL surface (i.e., there is a significant water/water interaction and not just a water/solid one). This situation results in a larger wetted area (and wetted diameter) for a given droplet volume, and subsequently, a larger sliding angle as shown in Figure 5. The wetted diameter represents the diameter of the contact area between the liquid-water droplet and GDL surface.

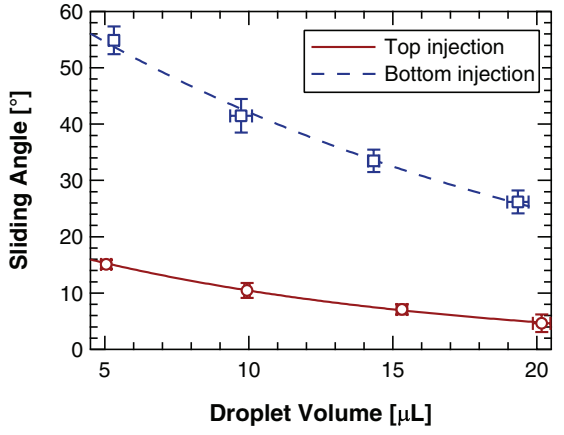

Figure 5. The dependence of the sliding angle on the injection method for SGL 24DA GDL. The symbols show the measured sliding angles for two injection methods as indicated in the legends, while the lines represent fitted exponential curves.

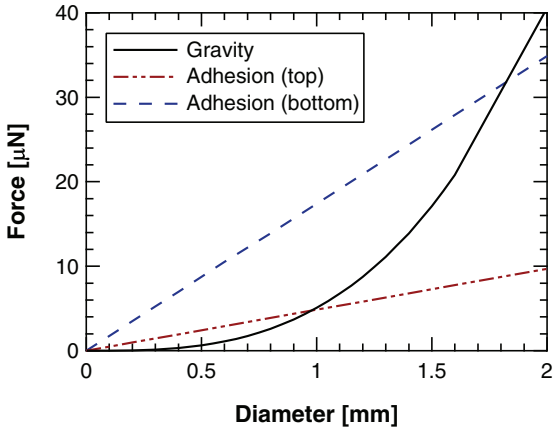

Figure 6. Variation of gravitational body force and total adhesion forces (with bottom injection) as a function of droplet diameter for droplets on SGL 24DA GDL.

The 'pinning' effect is found to be significant for the bottom injection, which assists the droplet adhesion with the GDL surface, whereas both the 'pinning' and 'dewetting' phenomena are present for a droplet placed on top of a GDL surface using the top injection. Here the pinning represents the scenario when the solid/liquid contact line remains pinned to the GDL surface while the liquid/gas interface shrinks, and the dewetting represents the scenario when the solid/liquid contact line shrinks with the liquid/gas interface. These effects are illustrated through the evaporation of a droplet on the GDL surface. Figure 7 shows the evaporation of a droplet on a SGL 24DA GDL (20-wt% Teflon loading) surface, and the pinning and dewetting phenomena with time for a droplet placed using the top injection as indicated in the figure. As observed, the change of the static contact angle (average of both the left and right contact angles) is non-uniform. It initially decreases due to evaporation, and it increases and then again decreases as the droplet size decreases due to evaporation. Here, the adhesion between the droplet and GDL surface changes with the droplet size, which influences the static contact angle. Clearly, the adhesion force dominates over the tension force that prevents the liquid-water droplet from contracting along the wetting line (for times less than 160 s). In other words, the pinning effect is dominant over the dewetting one. With the decrease of droplet size, the cohesion force eventually helps the droplet to contract, and the droplet exhibits the initial surface wettability again that is indicated between 160 s and 430 s in Figure 7c. As the droplet size further decreases, the adhesion force eventually regains its dominance, and the pinning effect is again observed after 430 s.

Unlike the above observations for a highly hydrophobic GDL, a low hydrophobic GDL, such as SGL 24AA (no Teflon loading), demonstrates that the pinning effect is significant for a droplet placed using top injection, as illustrated in Figure 8. Here, both the volume and static contact angle are monotonically decreasing due to the

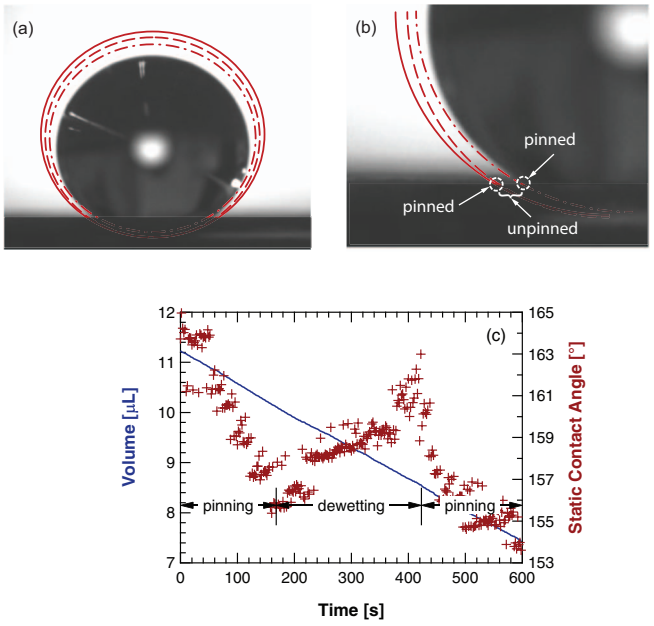

Figure 7. Pinning-dewetting phenomena of a liquid water droplet on SGL 24DA (20-wt% Teflon loading). The image in parts (a) and (b) shows the contraction of the droplet due to the evaporation after 10 min and the pinned and unpinned scenarios. The outer solid line in part (a) indicates the initial droplet size (initial liquid-gas interface), the dashed line indicates the shape after 2 min, and the dashed-dot line indicates the shape after 5 min. Part (c) shows the measured droplet volume (solid line) and static contact angle (symbols) as functions of time.

absence of the dewetting effect. Clearly, the results shown in Figures 5 thru 7 indicate that a GDL surface can exhibit higher adhesion forces depending on how the droplet is formed. In addition, the static contact angles are found to be strongly dependent on the droplet size and the static droplet on the GDL surface has inherent hysteresis. This finding is identical with the results available in the literature for solid surfaces,[37–39] and the droplet size effect on the contact angle is shown for the first time here for porous GDL surfaces. The inherent hysteresis as a function of Teflon loading is shown in Figure 9. Here, both the left and right contact angles are measured for static droplets on four different GDLs. For all the measurements, right and left contact angles are found to be different due to the surface and chemical heterogeneities.

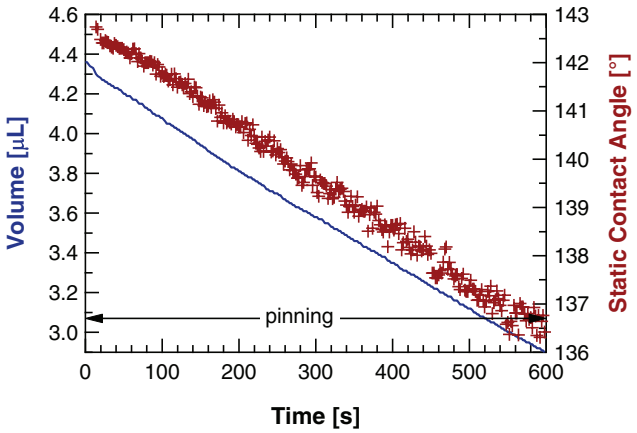

Figure 8. Illustration of pinning effect for liquid water droplets on SGL 24AA (no Teflon loading). The solid line shows droplet volume and the symbols depict the change of the static contact angle.

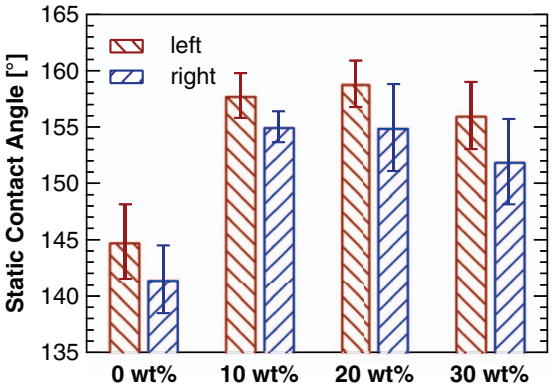

Figure 9. Measured static contact angle (both left and right contact angles) on a horizontal surface as a function of Teflon loading for SGL 24 series GDLs. The error bars indicate the standard deviations of the measurements.

Adhesion-force analysis.— The adhesion force between a droplet and GDL surface is calculated from the measured sliding angle, droplet volume, and wetted diameter using Eq. 2. The measured wetted diameters and the calculated adhesion forces between the liquid-water droplet and SGL 24DA GDL are shown in Figure 10 as a function of droplet volume for both the top- and bottom-injection methods. As expected, the adhesion force is independent of the droplet volume. The adhesion force between the liquid-water droplets and SGL 24DA are found to be 11.79 ± 0.23 mN/m and 3.28 ± 0.10 mN/m for bottom- and top-injection methods, respectively. The dependence of the adhesion force on injection method results in different droplet-detachment criteria of the same surface in different application areas. It is clear from the results shown in this section that both the sliding angle and adhesion force provide accurate identification of the GDL

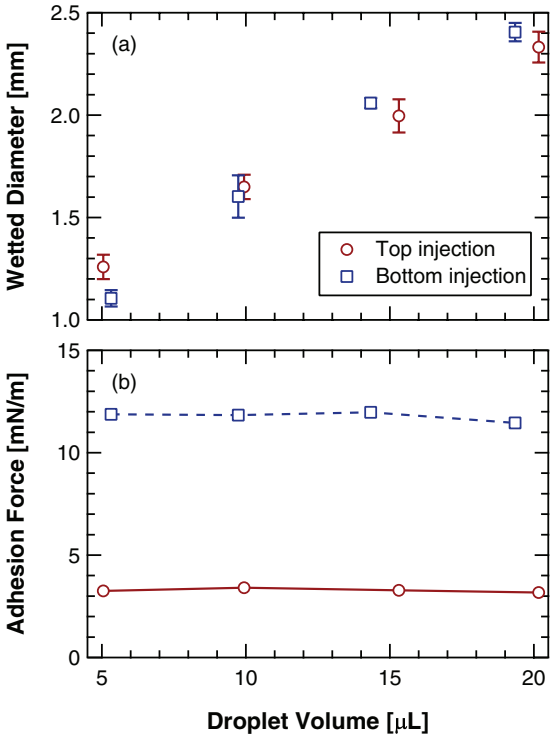

Figure 10. Wetted diameter (a), and adhesion force (b) between water droplet and SGL 24DA GDL as a function of droplet volume for top and bottom injections.

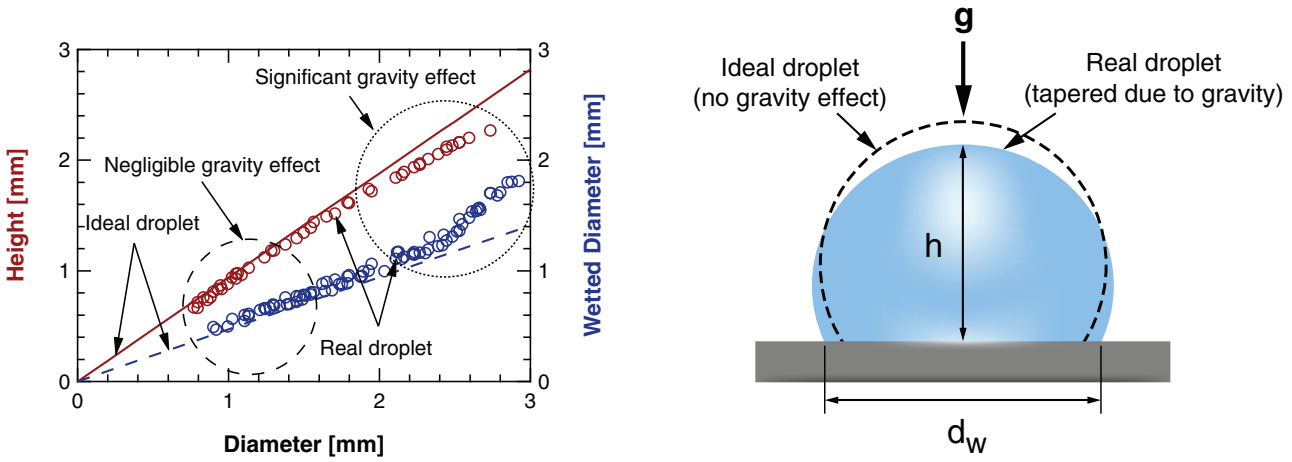

Figure 11. Effect of gravity on the droplet shape indicated by the deviation of droplet height (h) and wetted diameter (d_w) from ideal droplet's height and wetted diameter as a function of droplet diameter. The lines show the ideal droplet height (solid) and wetted diameter (dashed), the symbols show the measured data for SGL 24DA. The right part shows a schematic representation of the effect of gravity on an ideal droplet and a real droplet.

surface's wetting behavior that cannot be captured from contact angle measurements.

During the sliding-angle experiment, the effect of gravity on the droplet was also investigated in order to identify the droplet size limit for the sliding-angle measurements and to quantify the effect of gravity on the liquid-water removal for PEMFCs. The widely used approach to identify the effect of gravity on a sessile drop is based on the Bond number. The Bond number is a measure of the relative effects of gravitational and surface forces on the shape of a liquid surface, and the gravitational influence on the droplet shape may be neglected for systems when the Bond number is less than unity.[40] However, in this work, it is observed that the Bond number has to be significantly smaller than unity for GDL surfaces in order to neglect the gravity effect on the droplet shape. This is mainly due to the hydrophobic nature of the GDL surfaces; gravity will have a stronger influence on a given droplet on a hydrophobic than on a hydrophilic surface. The effect of gravity was explored by creating droplets on SGL 24DA with top injection and measuring its height, diameter, and wetted diameter as functions of droplet volume. The experimentally measured droplet height and wetted diameter are shown as a function of droplet diameter in the left part of Figure 11. Here, the symbols show the experimental data, while the lines depict the theoretical estimates for an ideal droplet (perfectly spherical). It is observed that the droplet height decreases and wetted diameter increases with the droplet diameter, and hence with the volume, compared with the ideal droplet's height and wetted diameter. These results indicate that as the droplet size increases the effect of gravity on the droplet also increases. A schematic of droplet deformation due to the gravity is shown in the right part of Figure 11. As indicated, the droplet's height decreases due to gravity compared with the height of a droplet with negligible gravity effect; the measured data (left part of Figure 11) also demonstrate the same trend. The results also elucidate that the effect of gravity on the droplet shape will be negligible of a droplet of diameter smaller than 1.5 mm on SGL 24DA (region indicated by the dashed circle) and the effect of gravity will be significant of a droplet diameter of 2.0 mm or larger (region indicated by the dotted circle). It should be noted that a droplet of 2.0 mm in diameter will have a Bond number of about 0.14. The data highlight the fact that care must be taken to account for the dependence of the droplet's wetted diameter and height (for droplets greater than 5 μL or 2 mm diameter on SGL 24DA), something that has been neglected in previous studies on droplet detachment.[16,17]

Typical PEMFC flow channels are around 1 mm. For a 1 mm flow channel, the largest single droplet will always be less than 1 mm, as it will completely block the flow channel. As shown in Figure 6, the adhesion force for a 0.5 mm droplet is almost an order higher than the gravity body force for bottom injection. Even for 1 mm droplet, the adhesion force is significantly higher than the gravity body force. Therefore, gravity should not influence the detachment of a single droplet for typical PEMFC operation, where the droplet size is always smaller than 1 mm. However, an agglomeration of droplets that forms a slug in the channel will eventually be significantly impacted by gravity.

Impact of injection rate.— The injection rate is critical to study as it is analogous to the operating current density in an operating PEMFC. An injection rate of 1 μL/s corresponds to a water flux out of the PEMFC cathode equivalent to a current density of 2.5 A/cm^2 assuming a beta value (net water transport coefficient in the membrane) of 0.5. The effect of injection rate on the sliding angle and adhesion force are shown in Figure 12 for a bottom injection. Here four different injection rates were used to create a 20 μL droplet. The sliding angle decreases with the injection rate, thereby indicating that the adhesion between the water droplet and GDL surface decreases with injection rate. In other words, faster injection enhances droplet detachment from the GDL surface. Although not shown, the static contact angle decreases with the injection rate, which results in a nonintuitive opposite trend in terms of adhesion force or wettability.

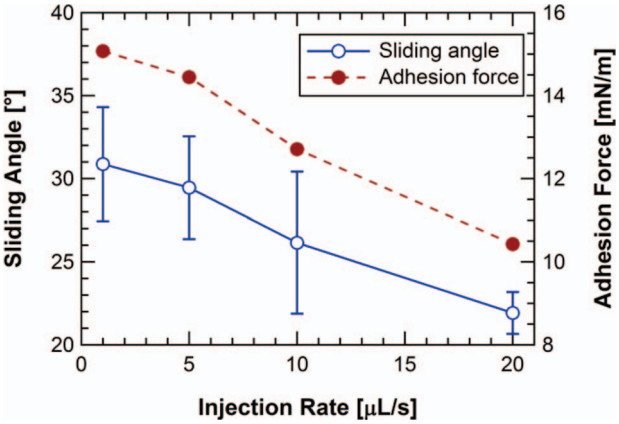

Figure 12. Effect of injection rate on sliding angle and adhesion force for SGL 24DA GDL with bottom injection.

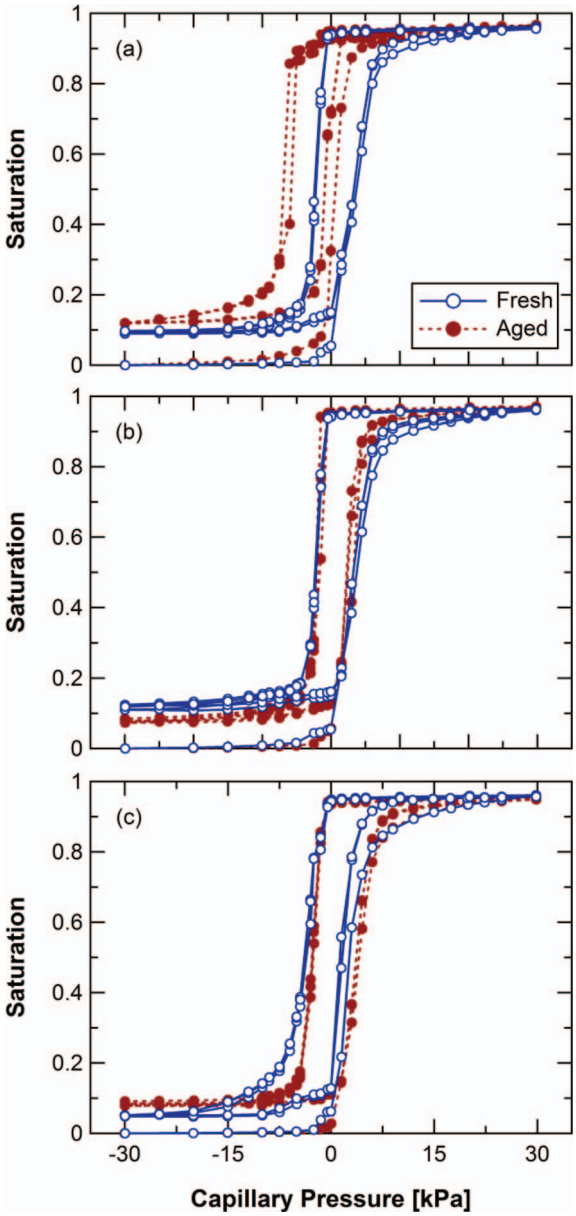

Figure 13. Saturation as a function of capillary pressure for both fresh and ex-situ-aged SGL (a) 24AA, (b) 24BA, and (c) 24DA GDLs.

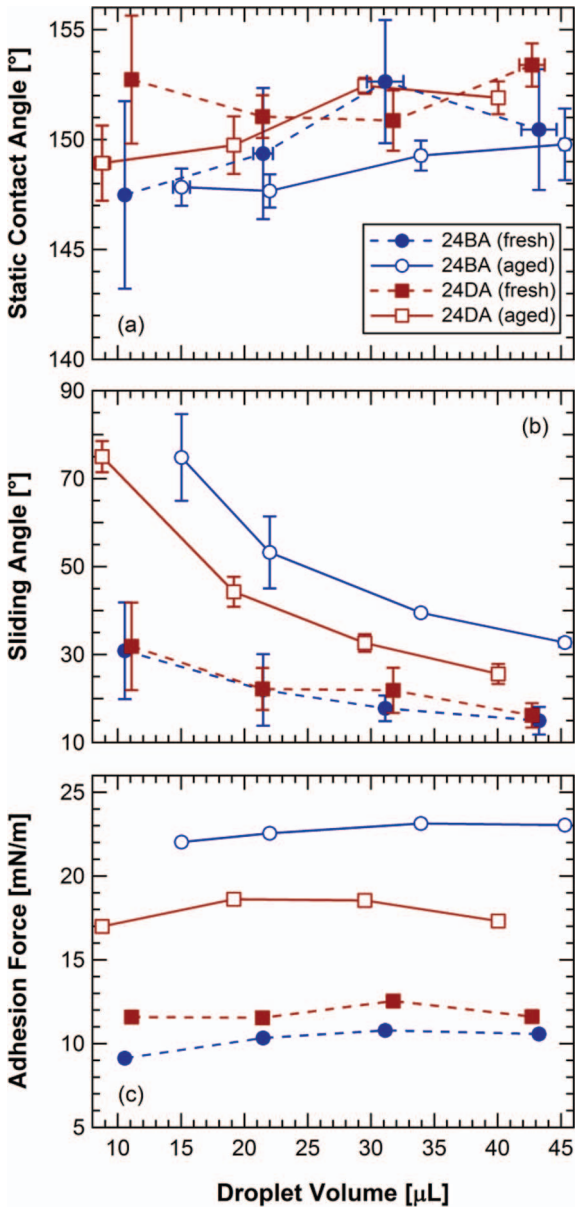

Figure 14. Comparison between fresh and aged GDLs through (a) contact angle and (b) sliding-angle measurements and (c) adhesion-force calculations as a function of droplet volume.

Impact of aging.— It is known that carbon-based materials become more hydrophilic as they age in a water or oxidative environment due to the formation of hydroxide, oxides, and other species on the carbon surface.[41] This has been seen in terms of PEMFC performance and components by Borup and co-workers.[42–44] It is thus worthwhile to examine how aging can impact the water properties of GDLs. For this analysis, SGL 24AA, 24BA, and 24DA GDLs were ex-situ aged by submersion in boiling 30% H_2O_2 solution for 7 hours. The aged samples were compared to fresh ones in terms of their capillary properties, contact and sliding angles, and adhesion forces.

The capillary pressure – saturation relationship for the tested GDLs is shown in Figure 13. The measurement was done according to the procedure in the literature.[45] The figure clearly shows that only the 24AA sample, which does not contain Teflon, shows any significant change in the hydrophobicity of the sample. In fact, once Teflon has been added, it appears that the bulk hydrophobicity of the sample does not change, which is not in agreement with the cell studies that show higher mass-transfer losses that stem from more water holdup within the cell.

Figure 14 shows contact-angle and sliding-angle data for the fresh and aged GDL samples with Teflon. The sample without Teflon, SGL 24AA, demonstrated a drastic increase in hydrophilicity as determined by both the sliding and contact angles; again demonstrating that some Teflon is required to retard the increased wettability of the bare carbon material, and in-agreement with the capillary-pressure-curve findings. As observed in Figure 14a, the average contact angle for the SGL 24DA is about 152° and 150.8° for fresh and aged GDLs, respectively, and for the SGL 24BA is about 150° and 148.6° for fresh and aged GDLs, respectively. These contact angle data indicate that a GDL's hydrophobicity decreases due to aging; however, the differences in contact angle are not statistically meaningful, especially since the droplet volume has an influence on the contact angle measurements.

Like the contact angles for SGL 24BA and SGL 24DA fresh samples, the sliding angles are almost identical and do not show any significant effect of the Teflon loading although SGL 24DA has twice

the Teflon loading than SGL 24BA. The sliding angles for SGL 24BA and SGL 24DA aged samples, however, do show a distinct difference not only with the aging, but also with the Teflon loading as shown in Figure 14b. The sliding angle data also reveal that the aging effect on GDL hydrophobicity is higher for SGL 24BA. Hence, the higher content of Teflon in a GDL retards the loss of hydrophobicity. The adhesion forces corresponding to these sliding angles are shown in Figure 14c. The adhesion forces are significantly higher for aged GDLs, which mean larger external forces will be required to remove water droplets. Although both fresh 24BA and 24DA GDLs show almost identical adhesion forces, the aged 24BA and 24DA GDLs show distinct adhesion forces. When combined with the capillary-pressure analysis above, these results demonstrate that aging seems to effect more the water removal rather than the intrinsic water interactions within the GDL. In other words, aging makes it harder to remove water and this increases the water holdup within the PEMFC, i.e., it is an interfacial- and not bulk-dominated phenomenon.

Conclusions

In this study, an experimental protocol has been described for measuring directly the adhesion force for liquid-water droplets on a proton-exchange-membrane fuel-cell gas-diffusion layer (PEMFC GDL). It has been observed that both the droplet creation method and the history of the GDL are important for droplet growth and detachment on a GDL surface. Furthermore, the top placement method commonly used is shown to underpredict the adhesion force in most cases compared to a water droplet generated by water moving through the GDL from the bottom, which is similar to actual physics during PEMFC operation. The combination of contact-angle hysteresis and static contact angle seem to be inadequate to provide an accurate estimate of the adhesion force due to inherent pinning and dewetting effects, particularly for SGL 24DA or highly hydrophobic GDLs. Higher injection flow rates resulted in lower adhesion forces, perhaps due to the kinetic effects and different water-transport pathways that have developed. In addition, ex-situ aging of the GDLs has a more significant impact on their water removal capability rather than their bulk water-uptake properties as long as a minimal Teflon treatment has been used.

Acknowledgments

This work was supported by the Assistant Secretary for Energy Efficiency and Renewable Energy, Office of Fuel Cell Technologies, of the U.S. Department of Energy under contract number DE-AC02-05CH11231 and by a CRADA Agreement no. LB08003874 between LBNL and Toyota Motor Company. The authors thank Los Alamos National Laboratory for providing aged GDL samples and Haluna P. Gunterman for helping capillary pressure – saturation measurements. P.K.D. gratefully acknowledges the support of a Natural Sciences and Engineering Research Council of Canada's Postdoctoral Fellowship. A.G. acknowledges the HHMI Science for Life Scholarship from the University of Florida.

References

1. D. M. Bernardi and M. W. Verbrugge, *AIChE J.*, **37**, 1151 (1991).
2. T. E. Springer, T. A. Zawodzinski, and S. Gottesfeld, *J. Electrochem. Soc.*, **138**, 2334 (1991).
3. A. Z. Weber, R. M. Darling, and J. Newman, *J. Electrochem. Soc.*, **151**, A1715 (2004).
4. A. Z. Weber and J. Newman, *J. Electrochem. Soc.*, **153**, A2205 (2006).
5. U. Pasaogullari and C. Y. Wang, *J. Electrochem. Soc.*, **151**, A399 (2004).
6. P. K. Das, X. G. Li, and Z. S. Liu, *J. Electroanal. Chem.*, **604**, 72 (2007).
7. P. K. Sinha, P. P. Mukherjee, and C. Y. Wang, *J. Mater. Chem.*, **17**, 3089 (2007).
8. P. K. Das, X. Li, and Z. S. Liu, *Int. J. Hydrogen Energy*, **35**, 2403 (2010).
9. A. Z. Weber, *J. Power Sources*, **195**, 5292 (2010).
10. P. K. Das, X. Li, Z. Xie, and Z. S. Liu, *Int. J. Energ. Res.*, **35**, 1325 (2011).
11. C. Y. Wang, *Chem. Rev.*, **104**, 4727 (2004).
12. A. Z. Weber and J. Newman, *Chem. Rev.*, **104**, 4679 (2004).
13. N. Djilali, *Energy*, **32**, 269 (2007).
14. F. Barbir and S. Yazici, *Int. J. Energ. Res.*, **32**, 369 (2008).
15. K. Jiao and X. Li, *Prog. Energ. Combust.*, **37**, 221 (2011).
16. K. S. Chen, M. A. Hickner, and D. R. Noble, *Int. J. Energ. Res.*, **29**, 1113 (2005).
17. E. C. Kumbur, K. V. Sharp, and M. M. Mench, *J. Power Sources*, **161**, 333 (2006).
18. A. Theodorakakos, T. Ous, A. Gavaises, J. M. Nouri, N. Nikolopoulos, and H. Yanagihara, *J. Colloid. Interf. Sci.*, **300**, 673 (2006).
19. F. Y. Zhang, X. G. Yang, and C. Y. Wang, *J. Electrochem. Soc.*, **153**, A225 (2006).
20. R. N. Wenzel, *Ind. Eng. Chem.*, **28**, 988 (1936).
21. B. He, J. Lee, and N. A. Patankar, *Colloids Surf., A*, **248**, 101 (2004).
22. A. B. D. Cassie and S. Baxter, *T. Faraday. Soc.*, **40**, 0546 (1944).
23. A. W. Neumann and R. J. Good, *J. Colloid. Interf. Sci.*, **38**, 341 (1972).
24. J. Drelich and J. D. Miller, *J. Colloid. Interf. Sci.*, **164**, 252 (1994).
25. D. Y. Kwok and A. W. Neumann, *Adv. Colloid Interface Sci.*, **81**, 167 (1999).
26. C. G. Furmidge, *J. Coll. Sci.*, **17**, 309 (1962).
27. E. Pierce, F. J. Carmona, and A. Amirfazli, *Colloids Surf., A*, **323**, 73 (2008).
28. D. Oner and T. J. McCarthy, *Langmuir*, **16**, 7777 (2000).
29. B. Krasovitski and A. Marmur, *Langmuir*, **21**, 3881 (2005).
30. E. B. Dussan and R. T. P. Chow, *J. Fluid. Mech.*, **137**, 1 (1983).
31. E. B. Dussan, *J. Fluid. Mech.*, **174**, 381 (1987).
32. E. B. Dussan, *J. Fluid. Mech.*, **151**, 1 (1985).
33. M. Sakai, J. H. Song, N. Yoshida, S. Suzuki, Y. Kameshima, and A. Nakajima, *Surf. Sci.*, **600**, L204 (2006).
34. S. Suzuki, A. Nakajima, K. Tanaka, M. Sakai, A. Hashimoto, N. Yoshida, Y. Kameshima, and K. Okada, *Appl. Surf. Sci.*, **254**, 1797 (2008).
35. T. Furuta, M. Sakai, T. Isobe, S. Matsushita, and A. Nakajima, *Langmuir*, **27**, 7307 (2011).
36. A. Winkleman, G. Gotesman, A. Yoffe, and R. Naaman, *Nano Lett.*, **8**, 1241 (2008).
37. J. Drelich, J. D. Miller, and J. Hupka, *J. Colloid. Interf. Sci.*, **155**, 379 (1993).
38. J. Drelich, *J. Adhesion*, **63**, 31 (1997).
39. S. Vafaei and M. Z. Podowski, *Adv. Colloid Interface Sci.*, **113**, 133 (2005).
40. J. S. Allen, *J. Colloid. Interf. Sci.*, **261**, 481 (2003).
41. K. Kinoshita, *Carbon: electrochemical and physicochemical properties*, John Wiley Sons, New York (1988).
42. D. Wood, J. Davey, F. Garzon, P. Atanassov, and R. Borup, in *206th Electrochemical Society Meeting*, Honolulu, Hawaii (2004).
43. D. Wood, J. Davey, F. Garzon, P. Atanassov, and R. Borup, in *208th Electrochemical Society Meeting*, Los Angeles, California (2005).
44. R. L. Borup, J. R. Davey, F. H. Garzon, D. L. Wood, and M. A. Inbody, *J. Power Sources*, **163**, 76 (2006).
45. J. T. Gostick, M. A. Ioannidis, M. W. Fowler, and M. D. Pritzker, *Electrochem. Commun.*, **10**, 1520 (2008).